

# Dynamical consequences of CDM merger trees

Xavier Hernandez and William H. Lee

*Instituto de Astronomía, Universidad Nacional Autónoma de México, Apdo. Postal 70–264, Cd. Universitaria, 04510 México D.F.*

8 November 2018

## ABSTRACT

Within the context of the standard structure formation scenario, massive present day elliptical galaxies are sometimes thought of as the result of a major merger of spiral systems. Through extensive SPH simulations of merging spirals, we have explored these processes with the aim of quantifying their relaxation times. This is important, as it sets a minimum time interval between the onset of a merger, and the appearance of an elliptical galaxy. We then compare this constraint with predictions of the hierarchical scenario, computed through Press-Schechter merger trees. We find evidence for elliptical systems which appear not to have been formed by a major merger of spirals.

**Key words:** galaxies: formation - galaxies: evolution - galaxies: elliptical and lenticular, cD - galaxies: interactions - cosmology: theory.

## 1 INTRODUCTION

In cosmology, the inflationary paradigm has not only provided an elegant answer to several disturbing problems of the standard Big Bang such as the horizon and the “flatness” problems, but also provides a mechanism for generating the primordial fluctuations from which we expect astrophysical structures to be formed. In most simple inflationary models, the initial spectrum of these fluctuations is a power law of the scale, and there is total absence of phase correlation among different scales. These properties lead to the hierarchical scenario of structure formation, where small scale objects merge continuously to produce increasingly larger ones as time goes by (e.g. White & Rees 1978; White et al. 1987).

The predictions of this model at large scale have been highly successful in matching the observed universe. N-body simulations of galactic clusters and super clusters match equivalent observed systems remarkably well. However, at galactic and sub-galactic scales considerable debate remains. Is the centrally concentrated dark matter density profile obtained from simulations of galactic dark haloes representative of the constant density cores seen in real galaxies or not (e.g. de Blok & McGaugh 1997; Firmani et al. 2001; Gnedin & Zhao 2002)? Is the level of substructure predicted by simulations at galactic levels compatible with the abundance of satellite systems in large galaxies, or are too many satellites being predicted (e.g. Moore et al. 1999; Ghigna et al. 2000)? Are the sizes of large disk galaxies compatible with the loss of angular momentum which models predict, mostly as a consequence of the extensive merging regime these systems should have been subject to, which should probably have

heated the disks beyond observed constraints (e.g. Navarro & Steinmetz 2000)?

It is clear that the assumptions going into the hierarchical model, at galactic and sub-galactic regions, remain subject to serious doubt. This is not surprising, since they result from large extrapolation of the direct analysis of primordial fluctuations performed at a much larger scale range, mostly through the study of the cosmic microwave background.

In this paper we shall examine another of the predictions of the hierarchical clustering scenario at the galactic level, namely the formation of massive elliptical galaxies through the merger of spiral systems. Examples of this proposal can be found in: Kauffmann (1996), Baugh et al. (1996), Somerville et al. (2001), Benson et al. (2002), Steinmetz & Navarro (2002) and Khochfar & Burkert (2003). That spiral galaxies sometimes collide and merge is an observational fact, that the remnant closely resembles an elliptical galaxy, has been proven repeatedly through numerical simulations, nevertheless the above do not constitute proof of the main formation mechanism for elliptical galaxies being through major mergers of spirals.

Through detailed Smooth Particle Hydrodynamics (SPH) simulations of the merger of two spirals, we will estimate the relaxation times for the process. Once this has been established, including a study of the variations expected given the extensive parameter space available to such a merger, and once the uncertainties in the initial conditions are considered, a consistency check for the hypothesis is available.

Simulations of galactic mergers have been carried out many times before, but mostly aimed at obtaining very particular information, and rarely situated in a cosmological context, as what we attempt here. For example, Hibbard &

arXiv:astro-ph/0210525v2 27 Oct 2003

Mihos (1995) explore merger remnant morphology and star formation, Barnes (2002) studies the formation of gas disks within merger remnants, Bendo & Barnes (2000) explore the distribution of line of sight velocities in merger remnants and remnant morphologies. Burkert & Naab (2003) study the process of elliptical galaxy formation through the merger of disks, but without including the dissipative gas component, an ingredient which we find here to be of relevance. We deemed it necessary to repeat the experiment, paying particular attention to setting up the initial conditions in a cosmologically justified manner, as well as exploring the explicit dependence of the final relaxation times on the ample configuration parameter space. For example, Ellis (2001) remarks on the necessity of cosmologically motivated merger simulations, to turn close galaxy pair statistics into merger rates.

Merger trees for large ellipticals can be constructed analytically, through the extended Press-Schechter formalism, and hence we have a prediction of the time elapsed between the last major merger and the present, for a galaxy of a given mass. This can be repeated, and given a redshift of observation, the hierarchical merger scenario predicts (on average) how far back in time the last major merger took place. This can be compared to the dynamical estimates of the relaxation time for the mergers. If the latter proves larger than the former, the theory needs revising.

In Section 2 we describe the numerical scheme used to model a collision between spiral galaxies, as well as the different configurations tested. Section 3 gives the results of the different simulations, giving the relaxation time criterion we wanted to establish. In Section 4 we calculate the Press-Schechter merger trees for elliptical galaxies, and compare to the relaxation time criterion of the previous section. Finally, our conclusions are given in Section 5.

## 2 MERGER SIMULATIONS

### 2.1 Numerical modeling

As stated in the introduction, we seek to obtain an estimate of the relaxation timescales for the merger of two spirals to result in a relaxed elliptical galaxy. Wanting to make a stringent comparison with models of structure evolution, we shall model the formation of a high redshift elliptical observed at  $z \sim 1.0$ . As we shall see, this implies starting the simulation at  $z \sim 1.5$ .

In attempting to model numerically the merger of two spiral galaxies, one must pay close attention to the gaseous component of the disk. It is this gas fraction through which most of the dissipation will take place, the other two components, stars and dark matter, being non-collisional. We hence used the method known as Smooth Particle Hydrodynamics (SPH), developed by Lucy (1977) and Gingold & Monaghan (1977), see Monaghan (1992) for a review. SPH is a Lagrangian method ideally suited for complicated three-dimensional flows, and has been used in a variety of astrophysical applications. We have specifically used the public code GADGET, developed by Springel et al. (2001) for galactic and cosmological simulations. This code allows us to trace shock fronts and other hydrodynamical features of the gas with great accuracy, as well as including an efficient

N-body routine, to follow the dynamics of the non-collisional components. Further the code is fully parallelized, allowing it to run on a large number of computers simultaneously, as was done in our case.

In setting up the spiral galaxies which are to collide, the first thing is to construct each galaxy in isolation. We include three components, a dark matter halo, a stellar disk and a gaseous disk, co-planar to the stellar one. In some variants, a stellar bulge was also added.

For the dark matter halo of each galaxy we chose a King sphere (King 1966). This has the advantage of including a fully self consistent distribution function, with the density profile being a solution to a Boltzmann and a Poisson equation. In this way we set up a “live” halo, which will respond to the formation of the disk in its centre and, as the galaxies approach, to tidal effects and all other dynamics of the merger. Although cosmological simulations (e.g. Navarro, Frenk & White 1996, Ghigna et al. 1998) result in dark matter halos which are much more centrally concentrated than King spheres, direct observations of Dwarf Irregulars and low surface brightness (LSB) galaxies seem to imply the existence of constant density cores in the centers of galactic dark matter halos (e.g. Burkert & Silk 1997; de Blok & McGaugh 1997), which are inconsistent with cosmological profiles, even taking into account possible expansions of the core due to efficient ejection of the central baryonic component (Gnedin & Zhao 2002) or observational effects (de Blok et al. 2003). In the dwarf spheroidals of the Milky Way, through velocity dispersion studies, Lokas (2002) finds that a core is statistically preferred to a cusp for the dark matter distribution, the same that results from a detailed galaxy velocity dispersion study in the Coma cluster (Lokas & Mamon 2003). The situation in clusters though, is not as clear as in galaxies, e.g. through strong lensing, Tyson et al. (1998) find that the dark matter halo in CL 0024+1654 is well represented by a structure having a central core, while van der Marel et al. (2000) find that CNOC1 redshift data for several clusters imply velocity dispersions and mass profiles consistent with NFW profiles.

Further, Hernandez & Gilmore (1998) showed that King halos produce rotation curves which are capable of matching both LSB and Dwarf Irregular and normal high surface brightness (HSB) observed rotation curves. Hernandez, Avila-Reese & Firmani (2001) also find strong evidence of a large constant density core in the dark matter halo of the Milky Way, in comparing the results of cosmological simulations of Milky Way formation, to extensive Galactic rotation curve determinations. Binney & Evans (2001) also find that detailed studies of the Milky Way rotation curve rule out an NFW type profile in our galaxy. Even in ellipticals, Romanowsky et al. (2003), through careful stellar kinematics, rule out the presence of dark matter to the extent implied by the cuspy NFW profiles. Since observational evidence in galaxies of all types favours dark halos with cores, it appears reasonable to model our galactic dark halos as King spheres. However, given the lack of a formation scenario to explain this observation, and given that the very successful hierarchical model implies cuspy halos, we included also one simulation using a cuspy NFW type halo.

King halos are defined by 3 parameters: the total mass of the halo, the total potential energy, and a shape parameter.

We take each of the dark haloes as having a velocity dispersion  $\sigma = 130 \text{ km s}^{-1}$ . A central density of  $\rho_0 = 0.02 M_\odot \text{ pc}^{-3}$  was assumed, in consistency with current estimates of this quantity obtained over a range of galactic systems (e.g. Firmani et al. 2000, Dalcanton & Hogan 2001, Shapiro & Ilev 2002, Lokas & Mamon 2003). We used a central potential in units of the velocity dispersion  $\Phi_0/\sigma^2 = 8.0$ , shown by Hernandez & Gilmore (1998) to result in optimal rotation curves, from LSB to HSB systems. We obtain a core radius  $r_c = 11.8 \text{ kpc}$ , a tidal radius  $r_{tidal} = 68r_c$  (where the density vanishes) and a total mass  $M_{halo} = 1.35 \times 10^{12} M_\odot$ . The halos were modeled out to 35 core radii, by which time 94% of the total mass of the halo has been included, and the dynamical times have become comparable to the Hubble time at  $z = 1.5$ .

For the stellar component we take a double exponential disk given by:

$$\rho(r, z) = \rho_*(0) \exp(-R/R_*) \exp(-|z|/z_*), \quad (1)$$

with the scale length,  $R_*$  fixed at 3.5 kpc, resulting in a  $\lambda$  parameter for the total galaxy of  $\sim 0.05$ . The vertical velocity dispersion for the stars was initially adjusted to yield a constant scale height of  $z_* = R_*/5$ . The normalization for the stellar disk was determined using a mass Tully-Fisher relation having a slope of 3.5, and normalized to the Milky Way (e.g. Giovanelli et al. 1997). When changes in the mass were explored, the disk scale lengths were scaled with the square root of the total disk mass, (e.g. Dalcanton, Spergel & Summers 1996; Avila-Reese, Firmani & Hernandez 1998), and the total disk mass scaled to the rotation velocity in the flat regime through the above mentioned Tully-Fisher relation.

The gas is initially distributed in an exponential disk having the same scale height as the stars, and a scale length equal to twice the stellar scale length, as normal spirals tend to show (e.g. Dalcanton et al. 1996). The normalization of the gas disk is fixed by requiring that  $M_g = F \times M_*$  i.e. that the total gas mass is  $F$  times the total stellar mass. Values of 0.3 and 0.5 were explored for this parameter, representing gas rich disks, as found by Mihos (2001b) to be typical of disk galaxies at  $z \sim 1$  in a  $\Omega_\Lambda = 0.7, \Omega_M = 0.3$  universe. Both the stars and gas are given a rotation velocity in the plane of the disk to balance the total gravitational inward pull, over which is added an isotropic velocity dispersion, as required by the vertical scale height criterion mentioned above.

GADGET uses an ideal gas equation of state,  $P = \rho u(\gamma - 1)$ , where  $u$  is the internal energy per unit mass, and  $\rho$  is the mass density. One can in principle introduce an atomic cooling law, and trace the detailed thermal evolution of the gas component. However, this results in catastrophic cooling and clumping of the gas. The above result is natural, when one considers that the energy content of gas in a galactic disk is heavily determined by the turbulent regime it is in. Once energy is found at the atomic thermal level, it is radiated away, for all practical purposes instantaneously. However, an extended “waiting phase” is implied by the large scale turbulence, which is also the phase into which much of the heating processes feed into. Supernova explosions deposit a large fraction of their energy into pushing and blowing the inter stellar medium around, rather than representing a co-

herent thermal heating mechanism (e.g. Mac Low & Ferrara 1999; Mori, Ferrara & Madau 2002).

With this in mind, one can try to model the turbulence, star formation, supernova explosions, and feedback mechanism between the above, to model the gaseous component of a galaxy. This not only very expensive computationally, but will probably also yield a wrong answer, given the lack of a detailed microphysics for star formation and turbulence. Theoretical models and direct observations of galactic disks suggest the existence of efficient feedback regulation mechanisms between star formation and turbulent dissipation, capable of maintaining the turbulent gas at the threshold for gravitational instability. Examples of the above can be found in Firmani, Hernandez & Gallagher (1996), Martin & Kennicutt (2001), and Silk (2001). In this sense, it appears reasonable to model the gas component of our galaxies through isothermal equations of state, assumed to be representative of the turbulent phase of the interstellar medium. Indeed, several authors have taken this approach in the modeling of gaseous components of galaxies (e.g. Barnes 2002; Athanassoula & Bureau 1999).

We have thus chosen to use an isothermal equation of state,  $P = c_s^2 \rho$ , where  $c_s$  is the sound speed. We incorporated the necessary changes to the code to make use of this, with  $c_s = 20 \text{ km s}^{-1}$  for most runs, and exploring the changes of this value on our final results.

We are hence assuming that heating processes, mainly shocks and supernova explosions at all times and at all places, exactly balance heat losses through viscous and turbulent dissipation. The above is well justified in isolated disks, were the gas naturally oscillates around the threshold of gravitational instability. In the more dynamic case of interacting and merging galaxies, the assumption breaks down whenever dynamical times become shorter than the 10 Myrs typical of the lifetimes of massive stars. This in effect sets a time resolution for our simulations, below which the details of our modeled mergers are probably unreliable. However, as our main aim is to obtain the timescale for the completion of the merger, this detail becomes of little relevance.

## 2.2 Initial conditions

Each of the galaxies which are to collide is set up as indicated in the previous subsection, with the stellar and gaseous disks introduced inside the equilibrium dark halo. This allows the dark halo to adjust to the presence of the disks, and it reacts by increasing the concentration of the inner regions slightly. The above initial disk conditions were chosen to guarantee also that the disks should be, in isolation, stable in terms of Toomre’s criterion, this was checked explicitly by evolving an isolated galaxy for 5 Gyr, no changes of any type were observed.

Figure 1 shows the radial profile of one of our galactic models at the start of the simulation. The vertical axis gives the actual rotation velocity in km/s, shown by the thin dotted curve, and the contribution to it of the dark matter halo given by the thin dashed line. The contribution of the exponential stellar disk is given by the solid curve, and that of the gas by the thick dashed one. This is seen to match inferences for the Milky Way quite well, outwards of about 3.5 kpc, (e.g. Kuijken & Gilmore 1989; Wilkinson & Evans 1999; Sakamoto et al. 2003). The inclusion of a stellar bulge

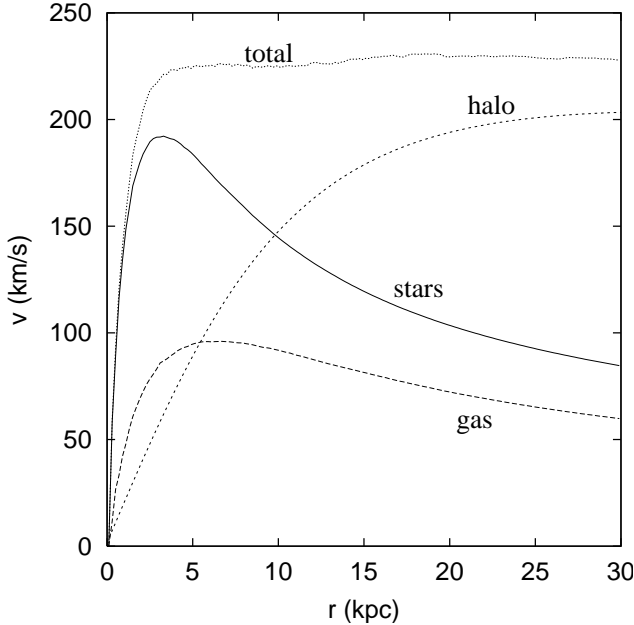


**Figure 1.** Rotation velocity curve, showing the total rotation curve as well as the contributions to this by the different components, in one of our modeled galaxies in isolation.

component, would in fact yield a much better agreement. In any case, our modeled galaxy is seen to reproduce observed systems quite well in having soft core dark halos, as commented in the previous subsection.

Once the disks are fully formed, the initial conditions for the dynamical evolution are established, and the merger is allowed to proceed. These initial conditions consist of a definition of the orbital plane for the encounter, an initial separation, an impact parameter, and the angular momentum vectors for the spins of the disks, defined in relation to the orbital plane.

The merger is clearly defined in a parameter space having several dimensions, the particular problem we are studying limits some of these, the remaining we shall explore by varying the relevant parameters.

In comparing with Press-Schechter merger trees, we have to define the start of the merger as the moment when the two galactic halos form part of a single bound structure. In this sense, it will be when the centers of both galaxies are four virial radii apart. This is based on the result (Padmanabhan 1995) of the turnaround radius of a fluctuation being equal to twice the virial radius, at any redshift.

Hence initially the galaxies, together with their corresponding DM haloes, are placed at a distance  $r_i = 4r_{\text{virial}}$ , where  $r_{\text{virial}}$  is computed for a single galaxy from:

$$\frac{3}{4\pi r_{\text{virial}}^3} \int_0^{r_{\text{virial}}} \rho dV = 200\rho(z_1), \quad (2)$$

where  $\rho(z_1) = \rho_0(1+z_1)^3$  is the critical density of the universe at redshift  $z_1$  (a generic redshift at which the merger starts) and  $\rho_0 = 3\Omega_M H_0^2 / (8\pi G)$  is its present value.  $r_{\text{virial}}$  is always smaller than the tidal radius of the halos, hence, the halos are fully sampled. We take  $z = 1.5$  and ( $\Omega_M = 0.3$ ,  $\Omega_\Lambda = 0.7$  and  $H_0 = 65 \text{ km s}^{-1} \text{ Mpc}^{-1}$ ), a present standard set of numbers to define our cosmological scenario.

The above defines the initial separations, as a function of the galaxies used. If one of the galaxies is taken at a different mass, the initial separation is adjusted so that the dark halos start off touching each other, in terms of their turnaround radii.

The orbital plane is arbitrarily taken as the XY plane, with the galaxies starting off with zero radial relative velocities. We are assuming they have just detached from the Hubble expansion, and only as they begin to feel each other gravitationally will they develop an infall radial velocity. The tangential velocity is specified through the total  $\lambda$  parameter for the full system, where:

$$\lambda = \frac{L|E|^{1/2}}{GM^{5/2}} \quad (3)$$

Here  $L$  is the total angular momentum,  $E$  the total potential energy of the system, and  $M$  the total mass. Given the cosmic distribution of  $\lambda$  parameters:

$$P(\lambda) = \frac{1}{\sigma_\lambda(2\pi)^{1/2}} \exp\left[\frac{-\ln^2(\lambda/\langle\lambda\rangle)}{2\sigma_\lambda^2}\right] \frac{d\lambda}{\lambda}, \quad (4)$$

with  $\langle\lambda\rangle = 0.05$  and  $\sigma_\lambda = 1.0$ , (e.g. Dalcanton et al. (1996) and references therein), we expect the total system to have been spun up by the surrounding tidal fields much to the same degree as individual galaxies have. Most of the simulations were run with an orbital  $\lambda$  of 0.05, with one test at 0.025 being included.

The remaining degrees of freedom in setting up the merger are related to the orientation of the disks with respect to the orbital plane. We could perhaps expect both disks to co-rotate with the orbit, as each was spun up by a similar tidal field in the surroundings of the forming binary system. However, the large stochastic nature of the acquisition of angular momentum in galaxies (e.g. Catelan & Theuns 1996) suggests that one is probably well advised not to assume any *a priori* orientations. We have tested 6 different configurations, specified by the arrows in the second column of Table 1, where the orbital angular momentum is up.

All other initial conditions of the runs are also summarized in Table 1. Run C0 corresponds to a configuration where the spin of both disks is aligned with the overall orbital motion. The orbital part of the dimensionless parameter  $\lambda$  is close to 0.05, as is that of all other runs, except for run C $\lambda$ , which is close to 0.025. The deviations from these two numbers are due to the different orientation of the individual spins, which however make up only a fraction of the orbital angular momentum. In runs C0 to C5 we have changed only the relative orientations of the two disks, with respect to the orbital plane, with the following 12 runs being variations of run C0 with changes in impact parameter, disk scale radii of the galaxies, the presence and mass of a bulge, the resolution of the simulation, the ratio of the masses of both systems, the gas fraction of the disks, the temperature of the gas disks, total mass of each galaxy, redshift at which the merger begins and adopted density profile for the DM halo.

### 3 RESULTS

We now examine in detail a series of merger simulations, representative of the many cases we explored. Figure 2 gives

**Table 1.** Basic parameters for each run. The table lists for each run (labeled) the initial spin configuration, the angular momentum parameter  $\lambda$ , the redshift  $z$  for which the initial condition was constructed, the total mass of the system (in units of the mass of a single “standard” galaxy, used for run C0), the gas fraction with respect to stars, the mass ratio  $q$ , the speed of sound  $c_s$ , the scale radii for the stellar disks, the presence of a massive stellar bulge (making up 50% and 70% of the stellar mass in cases Cb and CbM respectively), and the total number of particles used in the simulation,  $N = N_{halo} + N_{star} + N_{gas} + N_{bulge}$ . In all cases  $N_{halo}=20,680$ ,  $N_{gas} = N_{star} = 15,706$  and  $N_{bulge} = 0$ , except for run CN, where  $N_{gas} = N_{star} = 31,732$ , and run Cb, where  $N_{bulge} = 15,706$ . Run H0 is analogous to run C0, but used a Hernquist profile for the DM halo instead of a King profile (see text for details).

Run	Spins	$\lambda$	$z$	$M_t$	$M_{gas}/M_{stars}$	$q$	$c_s(\text{km s}^{-1})$	$R_{star}(\text{kpc})$	Bulge	$N$
C0	↑↑	0.082	1.5	2.0	0.5	1.0	20.0	3.50	no	52,092
C1	↑→	0.069	1.5	2.0	0.5	1.0	20.0	3.50	no	52,092
C2	↑↓	0.055	1.5	2.0	0.5	1.0	20.0	3.50	no	52,092
C3	↓↓	0.028	1.5	2.0	0.5	1.0	20.0	3.50	no	52,092
C4	↓→	0.043	1.5	2.0	0.5	1.0	20.0	3.50	no	52,092
C5	→→	0.061	1.5	2.0	0.5	1.0	20.0	3.50	no	52,092
Cλ	↑↑	0.060	1.5	2.0	0.5	1.0	20.0	3.50	no	52,092
CR	↑↑	0.069	1.5	2.0	0.5	1.0	20.0	1.75	no	52,092
Cb	↑↑	0.078	1.5	2.0	0.5	1.0	20.0	3.50	yes	67,798
CbM	↑↑	0.078	1.5	2.0	0.5	1.0	20.0	3.50	yes	67,798
CN	↑↑	0.082	1.5	2.0	0.5	1.0	20.0	3.50	no	84,144
Cq	↑↑	0.050	1.5	1.5	0.5	0.5	20.0	3.50	no	52,092
B	↑↑	0.078	1.5	2.0	0.3	1.0	20.0	3.50	no	52,092
Cc	↑↑	0.082	1.5	2.0	0.5	1.0	15.0	3.50	no	52,092
Cm	↑↑	0.083	1.5	1.0	0.5	1.0	20.0	3.50	no	52,092
Cmz	↑↑	0.075	2.5	1.0	0.5	1.0	20.0	3.50	no	52,092
Cz	↑↑	0.075	2.5	2.0	0.5	1.0	20.0	3.50	no	52,092
H0	↑↑	0.075	1.5	2.0	0.5	1.0	20.0	3.50	no	47,670

temporal snapshots (vertical sequence) of the evolution of simulations C0, C1 and C3, on the first, second and third columns, respectively. The times on the horizontal rows are the same, in all cases 3.53, 4.12, 4.7 and 5.3 Gyr. The dots show the stellar component of both disks, and the line contours give projected gas density plots, with the much more extended dark halo particles not being shown. The physical scale is 300 kpc on each side.

The uppermost frame in Figure 2 shows the onset of the collision, the first 3.5 Gyr are spent by the disks in falling into each other, from the initial condition at  $z = 1.5$ . In case C0 both disks co-rotate with the orbital spin, and hence are seen face on, as all frames show the galaxies on the orbital plane. The third column also shows the galaxies face on, as in this case both disks are counter-rotating with the orbit, evolution up until the disks interact is hence identical to case C0. The central column shows a simulation in which one of the disks spins perpendicular to the orbital plane, which is seen clearly in its first frame, where one of them is seen edge on.

By the second row the first encounter has taken place, and both disks are seen at maximum separation after the initial impact. At this stage the morphology of the interacting systems is heavily dependent on the initial conditions, with the large angular momentum of the disks in simulation C0 giving rise to two well defined tidal tails, both in the gaseous component (line contours) and in the stars (dots). The large degree of incoherence in the angular momenta of the two disks in the other two simulations shown leads to a significant canceling of this component, and both gas and stars form two tight knots.

By the third row significant dissipation has taken place, especially in the gaseous component where strong shocks and tidally induced features develop. This now forms a dense bar in the central regions of the remnant, no longer characterized by the double nucleus morphology seen previously.

A small tidal arm is seen in case C1, formed by gaseous and stellar material formerly associated to the co-rotating galaxy. By this time the differences between the three cases are beginning to fade. The final row shows the state of the remnants at the time when the temporal fluctuations in both total potential energies, total kinetic energies and isophote geometry disappear, and a final stable configuration is found. It is important to note that the total time for this to happen is the same for the three cases shown (see below).

Figure 3 is totally analogous to Figure 2, but shows the result of simulations C5, Cb and B, on the first, second and third columns, respectively. This explores the dependence of our results on yet another different orientation, both disks perpendicular to the orbital plane (C5). The other two examples use the relative orientation of case C0, but include the presence of a stellar bulge component in both galaxies, middle column, Cb, and a significantly different gas fraction of 0.3, in the third row, case B.

Again we see that the transition morphologies are highly sensitive to the initial conditions, with strong tidal arms developing in any component which co-rotates with the orbit, and falling rapidly towards the centre when this is not the case. However, the final relaxation times are again in excellent agreement with what was seen in the three cases shown in Figure 2, equilibrium configurations are attained by 5.3 Gyr in all cases. Other initial orientations listed in Table 1 give analogous results.

Inspection of the frames in Figures 2 and 3 reveals that the system has relaxed by approximately 5.2 Gyr. We proceeded to make a more thorough estimate of this timescale by analyzing the time evolution of various quantities for each simulation (all of them relating to the stellar component only). The first of these involves the eigenvalues of the inertia tensor. More specifically, we computed the square root of the ratios of these eigenvalues ( $R_1, R_2, R_3$ ), shown for

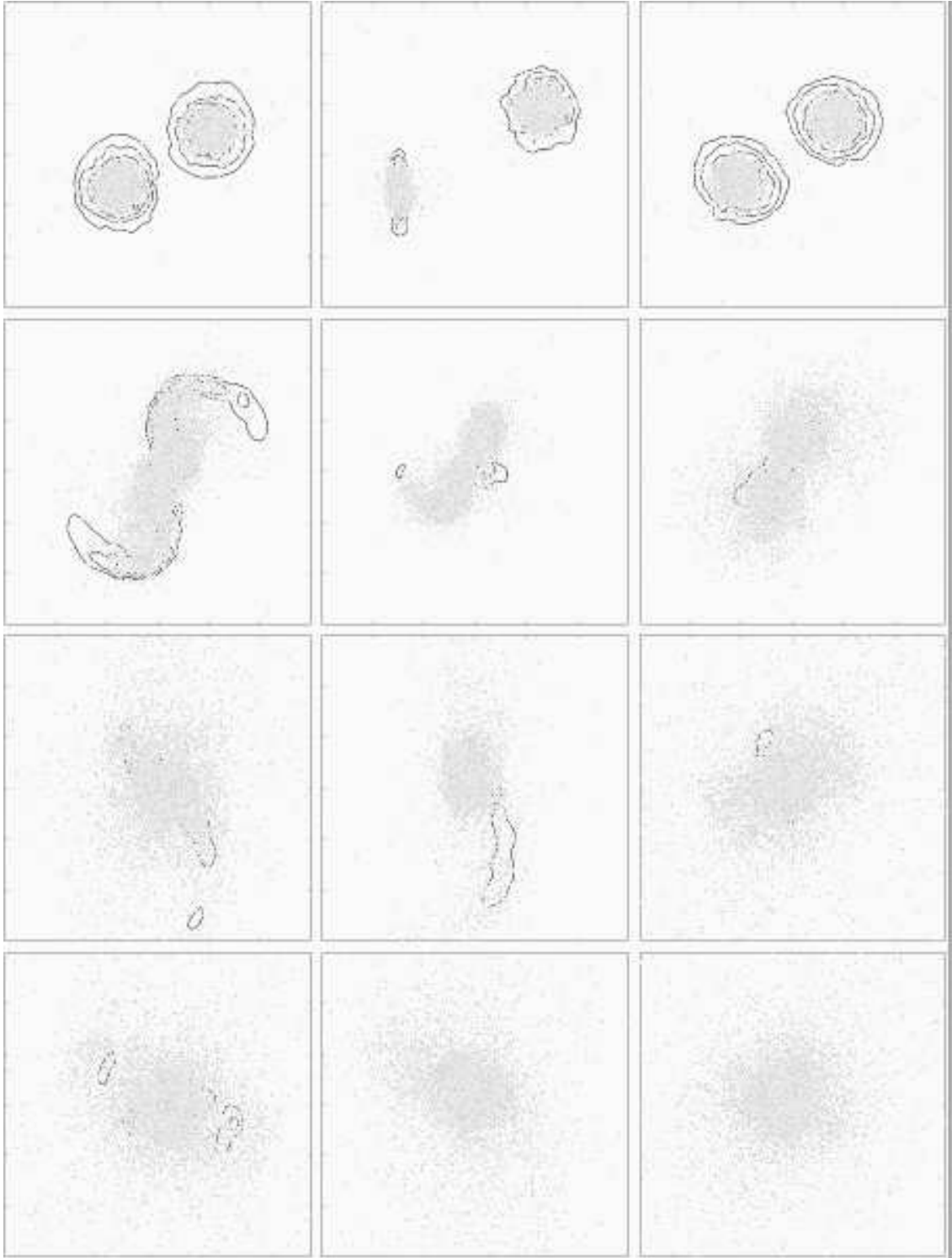


**Figure 2.** Snapshots of the dynamical evolution during the mergers for runs C0 (left), C1 (center) and C3 (right), in the orbital plane, at times  $t = 3.53, 4.12, 4.7, 5.3$  Gyr from top to bottom. The contours are logarithmic projected densities and equally spaced every 0.5 dex, with the lowest one at  $10^{-5} M_{\odot} \text{pc}^{-3}$ . The dots show the projected stellar particles. Each frame is 300 kpc on a side.

runs C0, C1 and C5 in Figure 4. This ratio is clearly a measure of the relative lengths of the principal axes of the mass distribution, and as such provides a good measurement of the overall shape of the system. The time variation clearly shows that the strongest fluctuations occur at the time of

the first collision, with the geometry settling down at around 5.0 Gyr. The degree of oblateness or prolateness is seen to depend on the initial conditions, particularly on whether the individual galaxies co-rotate with the infall orbit. We estimated a relaxation time from this information by defining

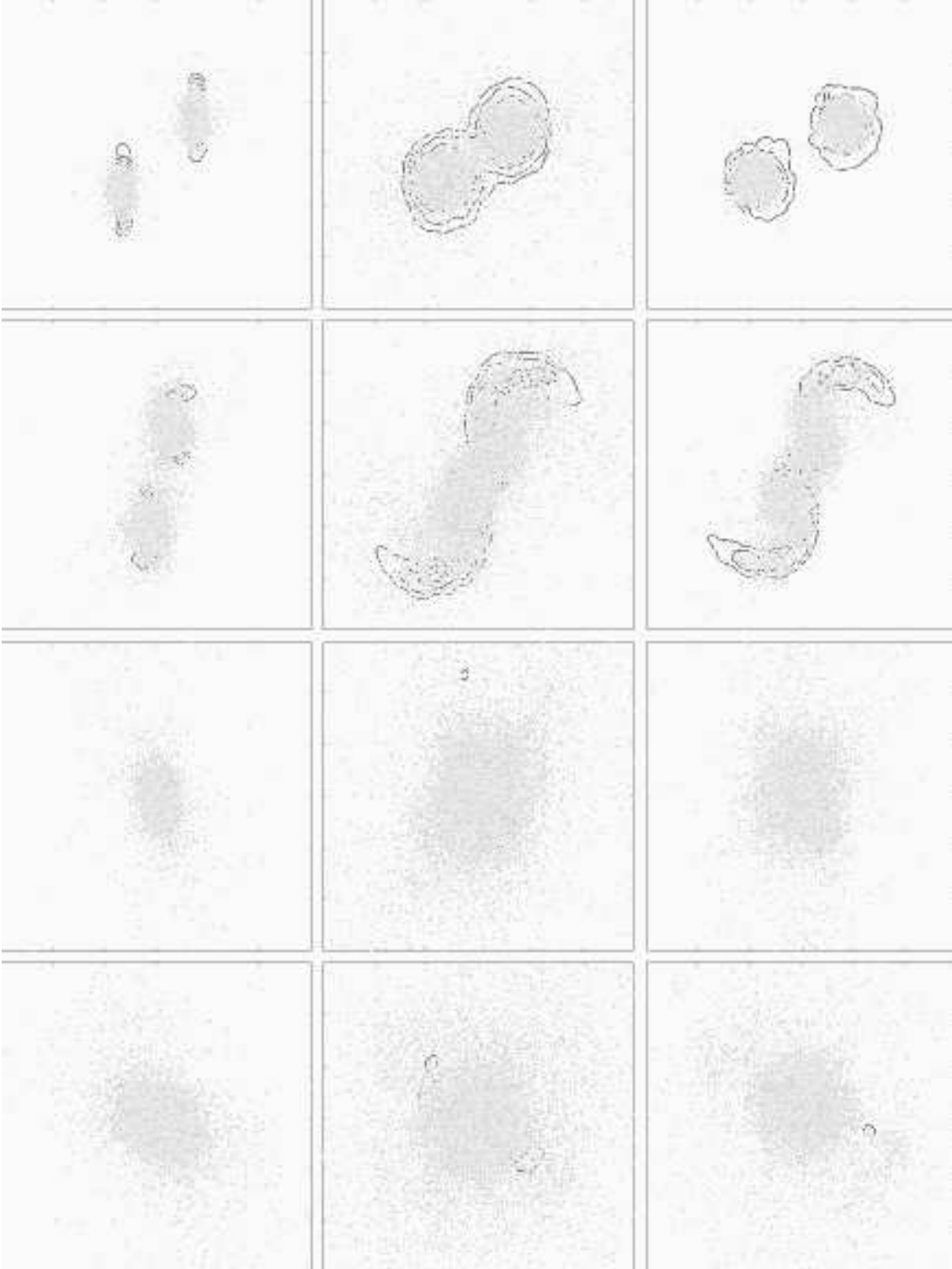


**Figure 3.** Snapshots of the dynamical evolution during the mergers for runs C5, Cb and B, in the orbital plane, at times  $t = 3.53, 4.12, 14.7, 5.3$  Gyr from top to bottom. The contours are logarithmic projected densities and equally spaced every 0.5 dex, with the lowest one at  $10^{-5} M_{\odot} \text{pc}^{-3}$ . The dots show the projected stellar particles. Each frame is 300kpc on a side.

$\tau_1$  as the time by which the fluctuations in the ratios  $R_i$  (sampled at intervals of 0.2 Gyr) had dropped below 5%.

The second quantity which we analyzed was the gravitational potential energy. Figure 5 shows its time evolution, both for the total value (bottom panel) and for the gas com-

ponent only (top panel), for runs C0, C1, C3, C5 and Cb, the first five of the cases shown in Figures (2) and (3). We note that an equivalent plot for the stellar components is very similar (albeit at a different absolute scale) than what is shown for the gas value. It can be seen that the details

of the first maximum/minimum in the energies vary slightly from case to case, but that in all cases no temporal oscillations remain beyond 5.3 Gyr. From the upper panel, it is clear that the dynamical relaxation timescales we adopt are representative of the process being modeled, and always fall within a narrow range of values, close to 4.8 Gyr. The sharp dip seen in the lower panel close to 4 Gyr shows the first collision, also seen as a sharp dip in the upper panel. However, the strong dissipation associated with breaking up the disks leads to a very strong loss of potential energy (particularly in the gaseous component) as the disks merge, not seen in the graph for the total energy, dominated by the massive dark halos, which essentially show a rebound.

In complete analogy with the determination of  $\tau_1$  described above, we defined  $\tau_2$  as the time by which fluctuations in the gravitational potential of stars had dropped below 5%, also sampled at intervals of 0.2 Gyr. Taken together, these quantities estimate both a dynamical relaxation ( $\tau_2$ ), and something closely corresponding to an “optical relaxation”,  $\tau_1$ . The global relaxation time was finally defined as  $\tau = \max(\tau_1, \tau_2)$ .

The relaxation times we find depend only weakly on the initial orientation of the disks, the details of the disk structure, and the physical conditions within them. This suggests that our final relaxation times are merely a dynamical result, expected to be a function only of the free-fall times at the initial conditions. This suggests a scaling with  $\tau \propto (1+z_1)^{-3/2}$ . We included simulation Cz to test this hypothesis, a case totally analogous to C0, but set up at  $z = 2.5$ . The results confirmed the scaling we expected, as did cases Cm (half the total mass at  $z = 1.5$ ) and Cmz (half the total mass at  $z = 2.5$ ). This allows us to express the total relaxation times of cosmologically constructed spiral galactic mergers as:

$$\tau_R = \frac{20.6 \pm 1.86}{(1+z_1)^{3/2}} \text{Gyr} \quad (5)$$

where  $z_1$  is the redshift at which the merger begins, and the range given shows a  $1\sigma$  variation which results from the range of values we found in the many experiments performed. We note that at the standard redshift  $z = 1.5$ , equation (5) gives  $\tau = 5.2 \pm 0.47 \text{Gyr}$

Although no explicit star formation has been introduced, in the interest of avoiding the introduction of free parameters pertaining to unknown physics, we do assume implicitly a certain degree of star formation, to justify the use of a constant gas temperature. Case Cc (where the speed of sound is  $c_s = 15 \text{ km s}^{-1}$ ) explores the sensitivity of our results to the actual value used for the gas temperature, and although intermediary morphologies are slightly affected, total relaxation times are not. Case CA was calculated to explore the effect of changing the impact parameter, in this case reduced by taking the orbital part of the  $\lambda$  parameter for the system at 0.025. Again, intermediary morphologies are affected, but final relaxation times are only slightly reduced, within the range of equation (5), as is the case with changes in gas and stellar disk scale radii (case CR) and mass ratio of the two galaxies (case Cq). Finally, case CN was a re-run of case C0, but at double the numerical resolution for the gas and stellar components. No differences were observed with respect to case C0, showing that our results are robust with respect to numerical effects. Additionally, one extra simulation, CbM tested whether including a very

massive bulge made a substantial difference. In this case, 70% of the mass in stars was included in the bulge, rather than in the more extended stellar disc. Thus in practice this simulation contained a rather massive, compact stellar core. our determinations of  $\tau$  were not affected beyond the values already established with the rest of the calculations.

Given that cosmological N-Body simulations yield dark matter halos having a much steeper central density profile than the king halos we used in most of our simulations (e.g. Navarro et al. 1996, Ghigna et al. 1998), we explore also the possible effects such a change in the dark halo might have on our results. Case H0 is completely analogous to case C0, but was calculated assuming a Hernquist profile (Hernquist 1990), having the same total mass. The scale parameter of the halo was adjusted so as to leave the rotation curves largely unchanged. Although the central dark matter densities in these cases were significantly larger than in the corresponding King halo ones, as the collisions get under way, first external and progressively more internal regions of the haloes begin to interact and merge. This implies disturbing the orbits of dark matter particles which make up the cusp, which is in turn dissolved fairly quickly. What we find is that this change produces only a marginal effect on the total relaxation times, which for case H0 fall within the distribution of relaxation times of the King halo cases, and indeed far from the extremes, which are due to extreme orientations of the disks, and values of the orbital  $\lambda$  parameter.

## 4 COMPARISON WITH HIERARCHICAL MERGER TREES

### 4.1 Analytical formulation of the problem

In the previous section the relaxation timescale of a merger has been established through dynamical simulations and cosmologically motivated starting conditions, as a function of the merger redshift. We now require an estimate of the formation timescale within the hierarchical clustering scenario. This will be done in a rigorous fashion by constructing merger trees within the extended Press-Schechter formalism, including all the cosmological details. However, before doing this it is convenient to derive an approximate analytical solution, valid only in the simple  $\Omega_M = 1, \Omega_\Lambda = 0.0$  scenario, and subject to numerous simplifying assumptions. This is done to obtain a clear understanding of the physics of the problem, and to provide an order of magnitude estimate to the trends and values one should expect in the more rigorous numerical experiments.

The mass function of progenitors of an object existing at  $z = z_o$  with mass  $M_o$ , viewed at  $z = z_1$  will be given by:

$$P(M_1) = \frac{M_0}{(2\pi)^{1/2}} \frac{\delta_c(z_1 - z_0)}{(S_1 - S_0)^{3/2}} \exp \left[ \frac{\delta_c^2(z_1 - z_0)^2}{2(S_1 - S_0)} \right] \left| \frac{dS_1}{dM_1} \right| \quad (6)$$

In the above equation  $P(M_1)$  is the probability of finding a progenitor of mass  $M_1$ , at  $z = z_1$ , where clearly  $z_1 > z_0$  (e.g. Lacey & Cole (1993); Nusser & Sheth (1999); Hernandez & Ferrara (2001)).  $\sqrt{S_i}$  is the rms density fluctuation in a top hat window function of radius  $(3M_i/4\pi\rho_0)^{1/3}$  and  $\delta_c$  the critical over-density for collapse, with  $\rho_0 = 3\Omega_M H_0^2/8\pi G$  being the present mean mass density of the universe.

As an example, Figure 6 shows the mass function which



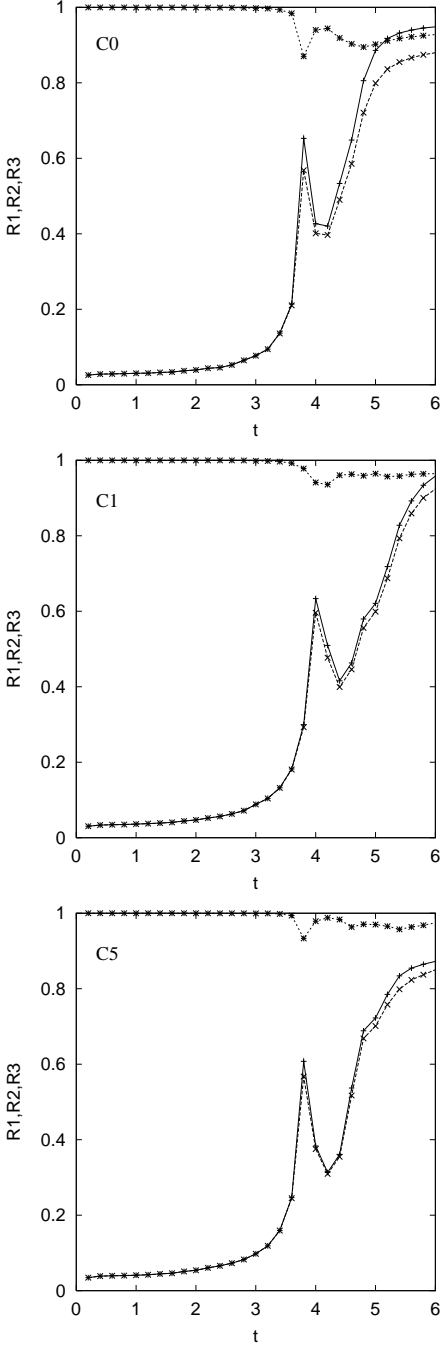


**Figure 4.** Time evolution of the ratios of the principal axes of the inertia tensor of the stellar component for (a) run C0, (b) run C1 and (c) run C5.

results from having “factored out” an observed object of mass  $M = 10^{12} M_{\odot}$ ,  $z_0 = 1.9$ , amongst its progenitors at various higher redshifts,  $z = z_1$ . This figure was calculated within a full  $\Lambda$ CDM scenario, the results for a simplified cosmology being qualitatively identical. We see that as  $z_1$  approaches  $z_0$ , the mass function of progenitors tends to a delta function at  $M_1 = M_0$ , as was to be expected. At progressively higher redshifts, the mass functions are characterized by very well defined maxima, which shift to pro-

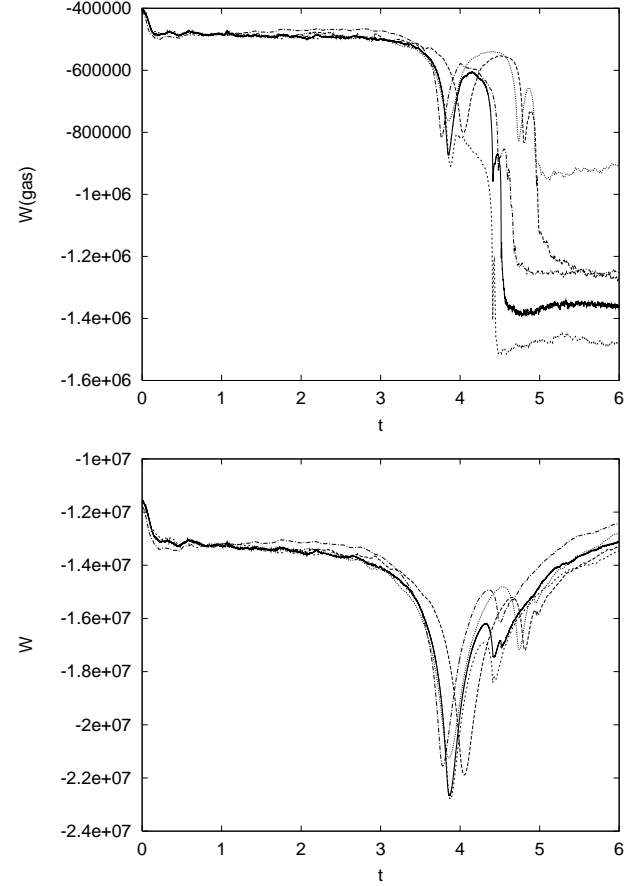


**Figure 5.** Gravitational potential energies as a function of time for runs C0, C1, C3, C5, and Cb (from top to bottom at the right end of the figure, respectively), gaseous components, upper panel, and total, lower panel. Time is given in units of  $9.8 \times 10^8$  yr, energies in units of  $2 \times 10^{53}$  erg.

gressively lower masses (note the logarithmic scales on both axes). In this way, we see that for the above case, in going to redshifts  $\geq 3.9$  (dashed curve), the chance of finding a progenitor with a mass comparable to, say,  $M_0/3$ , sharply drops.

For the analytical calculation, we shall take a fixed  $\delta_c = 1.7$  and  $\Omega_M = 1.0$ , as well as:

$$S(M_i) = S_8 M_i^{-1/3}, \quad (7)$$

valid for an effective spectral index in the galactic region of  $n = -2$ , where  $S_8$  is a normalizing factor to be fixed later (e.g. Padmanabhan 1995).

The idea now is to identify the redshift  $z_{1Max}$  which corresponds to  $dP(M_1)/dM_1 = 0$  evaluated at  $M_1 = M_0/2$ , as the redshift interval previous to  $z_0$ , during which a major merger might have formed the object  $(M_0, z_0)$ , as further back in the past of this redshift, the chances of finding a progenitor having half the mass of the observed object drop abruptly.

Substituting the power law dependence for  $S(M_i)$  in the rather cumbersome expression for  $dP(M_1)/dM_1 = 0$ , evaluated at  $M_1 = M_0/2$  yields:

$$(z_1 - z_0) = \frac{1}{\delta_c} \left( \frac{S_8}{M_0^{1/3}} \right)^{1/2} \quad (8)$$

We can now evaluate  $S_8$  from  $S_8 M_8^{-1/3} = 1$ , with:

$$M_8 = \frac{4\pi}{3} (8 \times 10^3 \text{ kpc})^3 \rho_c, \quad (9)$$

yielding:

$$S_8 = 8 \times 10^4 \Omega_M^{1/3}. \quad (10)$$

i.e., a  $\sigma_8 = 1$  normalization for the spectrum.

Substituting this last result, and the numerical value for  $\delta_c$  into equation (8) yields,

$$\Delta z_M = 166 \left( \frac{\Omega_M}{M_0} \right)^{1/6} \quad (11)$$

The above expression gives the redshift interval, backwards of a redshift of observation,  $z_0$ , beyond which it is unlikely that a major merger could have occurred, resulting in the observed object of mass  $M_0$ , and defines the merger timescale. It is interesting that in the simplified cosmology taken for this calculation, no explicit dependence on  $z_0$  remains.

Given that the initial conditions for the merger occurring at  $z = z_1$  require that the two galaxies be placed at a separation of a multiple of their current virial radii, the relaxation timescale,  $\tau_R$  will be estimated here as a multiple  $\alpha$  of order unity of the free fall timescale for a system having 200 times the background density of the universe. hence,

$$\tau_R = \left( \frac{3\pi\alpha}{32} \right)^{1/2} \left( \frac{1}{200\rho_0 G} \right)^{1/2} (1 + z_1)^{-3/2} \quad (12)$$

Introducing numerical values, and using  $t_H = (2/3)H_0^{-1}$  for the present age of the universe gives:

$$\tau_R = 0.17\alpha \frac{t_H}{(1 + z_1)^{3/2} \Omega_M^{1/2}} \quad (13)$$

Before comparing the above relation to the merger timescales of equation(11), we shall use:

$$1 + z_i = t_H^{2/3} t_i^{-2/3} \quad (14)$$

to arrive at:

$$166 \left( \frac{\Omega_M}{M_{Lim}(z_0)} \right)^{1/6} = (1+z_0) \left[ \left( 1 + \frac{0.17\alpha}{\Omega_M^{1/2}} \right)^{2/3} - 1 \right], \quad (15)$$

for the mass  $M_{Lim}(z_0)$  which at  $z = z_0$  has a merger timescale equal to the relaxation timescale at the point at which the merger began. Introducing  $\Omega_M = 0.3$  and  $\alpha = 1.6$  yields:

$$M_{Lim}(z_0) = 6.4 \times 10^{15} (1 + z_0)^{-6} M_\odot. \quad (16)$$

The above equation implies that at each redshift  $z_0$ , there should be a maximum limit mass above which an observed system could not possibly look like a relaxed elliptical galaxy, as then the relaxation timescale becomes longer than the merger timescale, and the object should look like an interacting system. One can note that this holds even at  $z = 0$ , however, at a fairly large total mass of  $6.4 \times 10^{15} M_\odot$ , which should be divided by a factor of about 20 to obtain stellar masses. Still, this limit mass is seen to fall very rapidly as  $(1 + z_0)^{-6}$ , and for example, for  $M = 2 \times 10^{12}$  —in the range

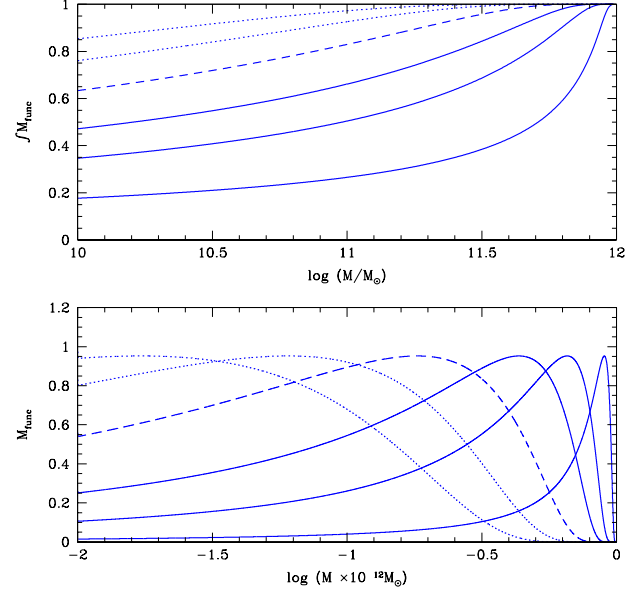


**Figure 6.** Lower panel: Mass functions of progenitors of a  $10^{12} M_\odot$  system, observed at  $z = 1.9$ , at different previous redshifts: 2.4, 2.9 and 3.3, (solid curves), 3.9, (dashed curve), and 4.5 and 5.1 (dotted curves). All curves have been normalized to 1. Upper panel: Integral of the mass functions shown in the lower panel. It can be seen that for redshifts higher than 3.9 (dotted curves), the chances of obtaining one progenitor with a mass of  $0.3 \times 10^{12} M_\odot$  or larger, drop below 5%, with the probability of two such fragments occurring being well below 0.25%.

of estimates for the mass of our Galaxy (e.g. Wilkinson & Evans 1999)— we arrive at  $z_0 = 2.8$  as the limit beyond which elliptical galaxies of that mass cannot be explained as having originated in a major merger. The choice of  $\alpha$  was motivated by the results of the simulations performed here, and that of  $\Omega_M$  by an attempt to come closer to a more realistic  $\Lambda$ CDM scenario. This last choice introduces a degree on inconsistency in the above calculation, which is only valid for  $\Omega_M = 1$ . However, as this is only intended as a conceptual guide, the result is probably a good first approximation.

## 4.2 Full $\Lambda$ CDM comparisons

We shall now turn to more precise numerical calculations, the results of which can be understood more clearly by using the above results as a conceptual guide, and an order of magnitude estimate.

The lower panel of Figure 6 gives the mass functions of progenitors of an object of total mass  $10^{12} M_\odot$ , observed at  $z_0 = 1.9$ , at various higher redshifts  $z_1 = 2.4, 2.9$  and  $3.3$  (solid curves),  $3.9$  (dashed curve), and  $4.5$  and  $5.1$  (dotted curves). This time the calculation was performed numerically evaluating equation (6) using a full  $\Lambda$ CDM scenario, with a fluctuation spectrum taken from Percival & Miller (1999). These curves are characterized by a maximum located at a value of the fragment mass which is a monotonically decreasing function of redshift. In this way, if the redshift at which the mass function of progenitors is calculated

is close to the redshift of observation, the mass function becomes increasingly dominated by an object having a mass very close to that which the object has at  $z = z_0$ .

At redshifts much higher than the observation redshift, the mass function becomes dominated by progenitors having only a few hundredths of the mass of the observed object, e.g. the dotted curves for  $z_1 = 4.5, 5.1$ . It is clear that if we want to form the  $10^{12} M_\odot$ , observed at  $z_0 = 1.9$  from a major merger, this cannot have taken place at such high redshifts. The solid curves show that this hypothetical major merger could well have taken place at a redshift of 2.4, 2.9 or 3.3, as at these values the mass function of progenitors for our  $10^{12} M_\odot$ ,  $z_0 = 1.9$  object includes a high probability of finding objects in the  $(0.3 - 1.0) \times 10^{12} M_\odot$  range. This is clearly seen in the top panel, where curves corresponding to those of the bottom one give the integrals of the mass functions, normalized to 1.0, and hence the functions to be sampled if the progenitors of our test object are to be obtained, at any of the previous redshifts shown.

Although the mass functions at  $z_1$  of 2.4, 2.9 or 3.3 do imply a high probability of finding progenitors in the ‘‘major merger’’ range, we cannot say that if the object  $10^{12} M_\odot$ ,  $z_0 = 1.9$  is an elliptical galaxy it was formed by a major merger having occurred in this redshift range. This is because in this redshift range, equation (5) implies that the relaxation timescale for such a merger,  $\tau_R(z_1)$ , is larger than the time intervals between any of those redshifts and  $z_0 = 1.9$ . This shows that if a major merger occurred between  $z_1 = 1.9$  and  $z_1 = 3.3$ , the result at  $z_0 = 1.9$  would be an interacting system, and not a relaxed elliptical galaxy. In fact, for this system, only just at the redshift  $z_1 = 3.9$ , corresponding to the dashed curve, does the relaxation timescale become equal to the time interval  $z_0 - z_1$ . This redshift  $z_1 = 3.9$  also corresponds to the maximum redshift out to which there is some chance of obtaining a progenitor in the major merger range, defined as at least a 5% chance of obtaining one progenitor with a mass upwards of 0.3 times the mass at the observation redshift. This condition defines the merger timescale,  $\Delta t_M$ , which in this case is equal to  $\tau_R$ .

In this way, we identify the observation redshift of  $z_0 = 1.9$  as the maximum redshift at which an elliptical galaxy of mass  $10^{12} M_\odot$  can be observed, if it is to be thought of as having been formed by a major merger. Smaller observation redshifts at this mass result in cases where  $\tau_R < \Delta t_M$ , and hence suitable candidates for a major merger origin, if they are elliptical galaxies. On the other hand, larger observation redshifts at this mass satisfy the condition  $\tau_R > \Delta t_M$ , and would therefore look like interacting systems, if formed by a major merger.

We can now repeat the calculation, and look for the limit observation redshift,  $z_{olim}(M)$  above which the major merger scenario fails for elliptical galaxies, as a function of total mass. This was done in constructing Figure 7, which shows  $z_{olim}(M)$ , as a function of mass, solid curve. The dotted curves represent our intrinsic uncertainty range for this quantity, given the variety of relaxation timescales we obtained, for the large range of orientations, dark matter profiles, orbital  $\lambda$ s and disk physics considered. Benson et al. (2002) reach a simplified version of our criteria, in requiring more than 10 relaxation timescales to have elapsed between the formation and observation of high redshift elliptical sys-

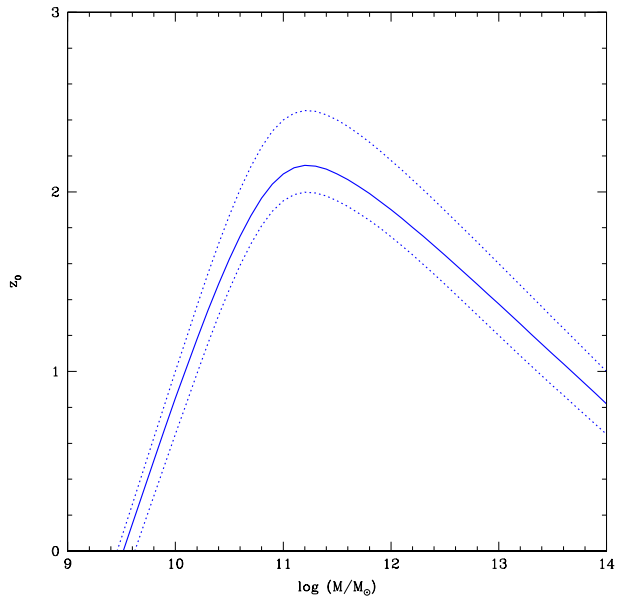


**Figure 7.**  $z_{olim}(M)$ , the maximum observation redshift at which an elliptical galaxy of total mass  $M$  can be thought of as having been formed as the result of a recent major merger.

tems, for colour and colour gradients data to be consistent with the hierarchical scenario.

## 5 CONCLUSIONS AND DISCUSSION

In considering our results of Figure 7 we firstly note that the expected scaling obtained for the simple analytic case is found only at high masses, where the curve of  $z_{olim}(M)$  does indeed tend to a  $M^{-1/6}$  scaling. However, the slight curvature found in the more realistic power spectrum, together with the high structure formation redshift in the  $\Lambda$ CDM scenario, result in a downturn at lower masses for this curve. This is interesting, as it establishes a maximum redshift of  $z_0 = 2.5$  above which any observed elliptical galaxy, whatever its mass, falls above the  $z_0 = z_{olim}(M)$  curve, i.e. in the  $\tau_R > \Delta t_M$  region. Any such elliptical galaxy would look like an interacting system, if it had formed as the result of a major merger.

Secondly we note that the region below the curve, where  $\tau_R < \Delta t_M$ , encompasses the majority of observed elliptical galaxies, which can hence be thought of as having been formed by the merger mechanism. However, the downturn at lower masses identifies a local maximum mass of  $1.3 \times 10^{10} M_\odot$  ( $6.3 \times 10^8 M_\odot$  in baryons), below which any observed ellipticals at any observation redshift  $z_0 > 1.0$ , must be thought of as having arisen through some mechanism distinct to the major merger hypothesis. The corresponding limit at  $z_0 = 0$  becomes  $3 \times 10^9 M_\odot$  ( $1.6 \times 10^8 M_\odot$  in baryons), comparable to the baryonic mass of many local dwarf ellipticals and larger than the few  $\times 10^7 M_\odot$  in baryons inferred for the dwarf spheroidal satellites of the Milky Way.

Again, we note the existence of a maximum redshift of  $z = 2.15 \pm 0.25$  beyond which all galaxies fall in the  $\tau_R > \Delta t_M$  region. A number of recent studies have shown

the existence of observed ellipticals in this region, inferred to be relaxed normal ellipticals though multi-wavelength studies of their stellar populations, or the normal appearance of their spectra. Studies of colours, luminosity function evolution, evolution (or lack thereof) of the fundamental plane zero point and clustering properties of high redshift ellipticals ( $1 < z < 3$ ) have shown that little evolution is seen to have occurred through merging over that period in field ellipticals, and that, at those high redshifts, most systems ( $\sim 70\%$ ) are already relaxed normal ellipticals, even considering problems related to dust obscuration, often at odds with the details of what the standard hierarchical scenario predicts e.g. Im et al. (1996), Moriondo et al. (2000), Daddi et al. (2000), Brinchmann & Ellis (2000), Daddi et al. (2001), Daddi et al. (2002), Cimatti et al. (2002), Im et al. (2002), and Miyazaki et al. (2002).

This last point forms our strongest conclusion. There is direct observational evidence for the existence of elliptical galaxies for which the condition  $\tau_R > \Delta t_M$  is met, and which within the hierarchical scenario of structure formation, in the observationally constrained  $\Lambda$ CDM scenario, (within the assumption of ellipticals forming in major mergers of spirals) should look like interacting systems, and not like relaxed elliptical galaxies at all.

It must be noted that we have used essentially present day galaxies and present day galactic scalings to model each of the spirals in the merger simulations. This is not entirely consistent, as our merger simulations take place at redshifts of 1.5 and 2.5. There is considerable evidence, both theoretical, within the framework of hierarchical structure formation models (e.g. Avila-Reese et al. 1998) and observational (e.g. Vogt 2001; Vogt & Phillips 2002) which implies very little or indeed no evolution of the mass Tully-Fisher relation with redshift. In this respect, the use of local values for this important structural relation for our high redshift galaxies is well justified.

The use of local disk scale length vs. disk mass relation however, is a different matter. Again both theoretical and observational studies of the redshift evolution of this scaling agree, giving a strong reduction in the disk scale length, in going to higher redshifts. This last point was not considered in most of our the simulations, because including it would only lead to longer relaxation timescales,  $\tau_R$ , and hence more dramatic, lower values of  $z_{olim}(M)$ , at all masses. This is clear if one considers that in reducing the typical sizes of disks, one is limiting the action and effects of the tidal forces which bring about dissipation and relaxation in the merging galaxies, as these dynamical effects scale with the size of the objects upon which they act. In a limiting case, one can imagine very small and compact disks which could be treated as point masses, the “merger” would not be more than the formation of a binary system in mutual orbit. Indeed, this effect starts to appear once the typical disk sizes become smaller than the distances of closest approach, relaxation times get longer and eventually tend to infinity, as the components become smaller. An analogous way of viewing this effect is to consider the typical density of the components. From a simplified classical tidal criterion, one can expect components to survive if their characteristic densities are higher than the average densities within their orbits. Indeed, our runs with shorter disk scale lengths yielded somewhat larger relaxation timescales.

It is hence clear that the use of local scaling laws leads to a conservative estimate of  $z_{olim}(M)$ , with results for a fully self consistent hierarchical scenario of structure formation yielding much more restrictive and lower values of  $z_{olim}(M)$ , at all masses. The same can be said of the lack of a specific recipe for star formation, the introduction of which would result in the conversion of gas into stars i.e. of a dissipative component into a non-collisional ingredient, hence lengthening the relaxation times. This last effect would be enhanced in the case of a starburst regime triggered by the pile up of gas in the central regions, and the subsequent loss of gas through a galactic wind, also increasing the fraction of the non-collisional stellar component.

Finally, we note that the arguments presented here are not the only objections that have been raised against the idea of all ellipticals being the result of major mergers. An early example mentioning many of the principal objections can be found in Ostriker (1980), who noted that the tight colour-magnitude and metallicity-magnitude relations seen in ellipticals would be hard to justify in a scenario dominated by the random assemblage of smaller spirals. He also pointed to the deeper potential wells found in ellipticals than in spirals, and the dissipationless nature of gravitational processes as a difficulty to this scenario, which also would have a hard time explaining the smaller physical scale lengths of ellipticals over spirals, since dissipationless mergers would tend to increase the scale of a system. Many of these objections have been stated again since in more careful terms, some examples follow.

Wyse (1998) has pointed out that the high phase-space density seen in elliptical galaxies and early bulges is incompatible with the formation of these systems out of the dissipational merger of stellar disks. This last point can be alleviated by the introduction of a dissipational component, such as the gaseous disk, coupled gravitationally to the stellar component. However, the very red colours of elliptical galaxies at high redshift limits the amount of gas that can be included in such a merger, the details depending on the efficiency with which a galactic wind could subsequently clear the merger of gas. Mihos (2001) finds that ellipticals which fall into anomalous places in the central parameter relationship invariably appear as merger remnants, and concludes that if mergers are the formation mechanisms for elliptical galaxies, these must have taken place at very high redshift. Interacting and starburst systems seen at moderate redshifts cannot form a significant fraction of the local elliptical population.

Mihos & Hernquist (1996) raise the problem of what happens to the gas in merging spirals, and point out that the extreme infall towards the centre seen in some simulations, if accompanied by in situ star formation, would result in light profiles for ellipticals which would be too centrally cusped to accommodate observed de Vaucouleur’s type profiles. Ellis et al. (2001b) find that the relative colours of bulges and ellipticals in the redshift range  $0.6 < z < 1.0$  are at odds with the predictions of the hierarchical scenario, suggesting very early formation epochs for ellipticals, or substantial “rejuvenation” of spiral bulges. Pozzetti et al. (2003) in fact, find that a careful study of the evolution of the K-band luminosity function agrees more with simple passive evolution models than with cosmologically motivated hierarchical clustering scenario of Kauffmann (1999). Firth et

al. (2002) conclude that the Las Campanas redshift survey rules out models where only passive evolution plays a part, but also that data are inconsistent with the low formation epochs of field ellipticals predicted in hierarchical scenarios. Birchmann & Ellis (2000) also note that the space densities of both large ellipticals and large spirals change very little out to  $z \sim 1$ , making it unlikely that large spirals are merging to form large ellipticals.

In going to spiral galaxies, studies of the velocity dispersion tensor in the Milky Way and other late type spirals e.g. Binney (2001) show that the lack of strong discontinuities in the vertical velocity of stars as a function of age appear to contradict the merger scenario, with dynamical heating by spiral arms being sufficient to account for the observations. Labbe et al. (2003) obtained deep imaging in the IR of HDFs objects, and found that 50% of the brightest objects, which in the optical show up as knotty mergers, are actually normal, relaxed large disks at  $1.4 < z < 3.0$

There seems to be mounting evidence pointing to a high formation redshift for ellipticals (and possibly also spirals), the results of our present study offering new support and being in accordance with the conclusions of a variety of independent studies centering on widely different aspects of the physics of the problem. If large ellipticals did not form out of the merger of comparably sized spirals, might they have formed out of the merger of comparably sized ellipticals? The relaxation timescales would be much longer than for the spiral mergers, as ellipticals lack the dissipative gaseous component, and have smaller sizes which make tides less relevant, making the problem we have pointed out in this paper worse. As alternatives we might think of many small spirals/ellipticals being swallowed by a growing elliptical system over a few Gyr period, provided most of the action ended before  $z \sim 2$ . It is perhaps time to consider what modifications are needed in the present galactic assemblage scenario in order to make it compatible with a high formation redshift for elliptical galaxies.

## ACKNOWLEDGMENTS

The authors wish to thank T. Padmanabhan and C. Firmani for helpful discussion, the Institute of Astronomy, Cambridge for its hospitality during the final phases of this work and the referee, Fabio Governato, for a detailed revision and helpful corrections which improved the final version. Support for this work was provided by CONACyT (27987E) and (I39181-E) and DGAPA-UNAM (IN-110600).

## REFERENCES

- Athanassoula E., Bureau M., 1999, *ApJ*, 522, 699  
 Avila-Reese V., Firmani C., Hernandez X., 1998, *ApJ*, 505, 37  
 Barnes J. E., 2002, *MNRAS*, 333, 481  
 Baugh, C. M., Cole, S., Frenk, C. S., 1996, *MNRAS*, 283, 1361  
 Bendo G. J., Barnes J. E., 2000, *MNRAS*, 316, 315  
 Benson, A. J. Ellis, R. S., Menanteau, F., 2002, *MNRAS*, 336, 564  
 Binney J. J., 2001, *ASP Conf. Ser.* 230, 33  
 Binney, J. J., Evans, N. W., 2001, *MNRAS*, 327, 27  
 Brinchmann J., Ellis R. S., 2000, *ApJ*, 536, L77  
 de Blok W. J. G., McGaugh S. S., 1997, *MNRAS*, 290, 533  
 de Blok W. J. G., McGaugh S. S., Rubin V. C., 2001, *AJ*, 122, 2396  
 de Blok W. J. G., Bosma A., McGaugh S., 2003, *MNRAS*, 340, 657  
 Burkert A., Silk J., 1997, *ApJ*, 488, 55  
 Burkert A., Naab T., 2003, *astro-ph/0305076*  
 Catelan P., Theuns T., 1996, *MNRAS*, 282, 455  
 Cimatti A., et al., 2002, *A&A*, 391, L1  
 Daddi E., Cimatti A., Renzini A., 2000, *A&A*, 362, L45  
 Daddi E., Broadhurst T., Zamorani G., Cimatti A., Rttgering H., Renzini A., 2001, *A&A*, 376, 825  
 Daddi E. et al., 2002, *A&A*, 384, L1  
 Dalcanton J. J., Hogan C. J., 2001, *ApJ*, 561, 35  
 Dalcanton J. J., Spergel D. N., Summers F. J., 1996, *ApJ*, 482, 659  
 Ellis R., 2001, *astro-ph/0102056*  
 Ellis R. S., Abraham R. G., Dickinson M., 2001b, *ApJ*, 551, 111  
 Firmani C., Hernandez X., Gallagher J., 1996, *A&A*, 308, 403  
 Firmani C., D'Onghia E. D., Avila-Reese V., Chincarini G., Hernandez X., 2000, *MNRAS*, 315, L29  
 Firmani C., D'Onghia E. D., Chincarini G., Hernandez X., Avila-Reese V., 2001, *MNRAS*, 321, 713  
 Ghigna S., Moore B., Governato F., Lake G., Quinn T., Stadel J., 1998, *MNRAS*, 300, 146  
 Ghigna S., Moore B., Governato F., Lake G., Quinn T., Stadel J., 2000, *ApJ*, 544, 616  
 Gingold R. A., Monaghan J. J., 1977, *MNRAS*, 181, 375  
 Giovanelli R., Haynes M. P., Herter T., Vogt N. P. 1997, *AJ*, 113, 22  
 Gnedin O. Y., Zhao H., 2002, *MNRAS*, 333, 299  
 Hernandez X., Avila-Reese V., Firmani C., 2001, *MNRAS*, 327, 329  
 Hernandez X., Ferrara A., 2001, *MNRAS*, 324, 484  
 Hernandez X., Gilmore G., 1998, *MNRAS*, 294, 595  
 Hernquist L., 1990, *ApJ*, 356, 359  
 Hibbard J., Mihos C., 1995, *AJ*, 110, 140  
 Im M., Griffiths R. E., Ratnatunga K. U., Sarajedini V. L., 1996, *ApJ*, 461, L79  
 Im et al., 2002, *ApJ*, 571, 136  
 Kauffmann, G., 1996, *MNRAS*, 281, 487  
 Kauffmann G., Colberg J. M., Diaferio A., White S. D. M., 1999, *MNRAS*, 303, 188  
 Khochfar, S., Burkert, A., 2003, *Ap&SS*, 285, 211  
 King I. R., 1966, *AJ*, 71, 64  
 Kuijken K., Gilmore G., 1989, *MNRAS*, 239, 571  
 Labbe I., et al., 2003, *ApJ*, 591, L95  
 Lacey C., Cole S., 1993, *MNRAS*, 262, 627  
 Lokas, E. L., 2002, *MNRAS*, 333, 697  
 Lokas, E. L., Mamon, G. A., 2003, *MNRAS*, 343, 401  
 Lucy L. B., 1977, *AJ*, 82, 1013  
 Mac Low M., Ferrara A., 1999, *ApJ*, 513, 142  
 van der Marel R. P., Magorrian J., Carlberg R. G., Yee H. K. C., Ellingson E., 2000, *AJ*, 119, 2038  
 Martin C. L., Kennicutt R. C., 2001, *ApJ*, 555, 301  
 McGaugh, S. S., Rubin, V. C., de Blok, W. J. G. 2001, *AJ*, 122, 2381  
 Mihos J. C., Hernquist L., 1996, *ApJ*, 464, 641  
 Mihos C., 2001, *ASP Conf. Ser.* 240, 143  
 Mihos C., 2001b, *ASP Conf. Ser.* 230, 491  
 Miyazaki et al., 2002, *astro-ph/0210509*  
 Monaghan J. J., 1992, *ARA&A*, 30, 543  
 Moore et al., 1999, *ApJ*, 524, 19  
 Mori M., Ferrara A., Madau P., 2002, *ApJ*, 571, 40  
 Moriondo G., Cimatti A., Daddi E., 2000, *A&A*, 364, 26  
 Navarro J., Frenk C., White S., 1996, *ApJ*, 462, 563  
 Navarro J., Steinmetz M., 2000, *ApJ*, 538, 477  
 Nusser A., Sheth R. K., 1999, *MNRAS*, 303, 179  
 Ostriker, J P., 1980, *ComAp*, 8, 177

- Padmanabhan T., 1995, *Structure Formation in the Universe*,  
Cambridge University Press, Cambridge
- Percival W., Miller L., 1999, *MNRAS*, 303, 179
- Pozzetti, L., et al., 2003, *A&A*, 402, 837
- Romanowsky A. J., Douglas N. G., Arnaboldi M., Kuijken K.,  
Merrifield M. R., Napolitano N. R., Capaccioli M., Freeman  
K. C., 2003, *astro-ph/0308518*
- Sakamoto T., Chiba M., Beers T. C., 2003, *A&A*, 397, 899
- Shapiro P. R., Iliev I. T., 2002, *ApJ*, 565, L1
- Silk J., 2001, *MNRAS*, 324, 313
- Springel, V., Yoshida, N., White, S. D. M., 2001, *New Ast.*, 6, 79
- Somerville R. S., Primack J. R., Faber S. M., 2001, *MNRAS*, 320,  
504
- Steinmetz, M., Navarro, J. F., 2002, *NewA*, 7, 155
- Tyson J. A., Kochanski G. P., dell'Antonio I. P., 1998, *ApJ*, 498,  
L107
- Vogt N. P., 2001, *Deep Fields*, ESO/ECF/STScI workshop, p.112
- Vogt N. P., Phillips A. C., 2002, *AAS*, 200 4008
- White S. D. M., Frenk C., Davis M., Efstathiou G., 1987, *ApJ*,  
313, 505
- White S. D. M., Rees M. J., 1978, *MNRAS*, 183, 341
- Wilkinson M. I., Evans W., 1999, *MNRAS*, 310, 645
- Wyse R. F. G., 1998, *MNRAS*, 293, 429